frontiers in Energy Research

ORIGINAL RESEARCH
published: 28 May 2021
doi: 10.3389/fenrg.2021.668111

Preparation of High-Performance Enteromorpha Prolifera–Based Porous Carbons by Nitrogen Modification and Their Electrochemical Performance

Ming Li, Kuihua Han, Zhaocai Teng, Meimei Wang, Yang Cao and Xian Li*

Shandong Engineering Laboratory for High-efficiency Energy Conservation and Energy Storage Technology and Equipment, School of Energy and Power Engineering, Shandong University, Jinan, China

This study presents a novel method to improve the electrochemical performance of porous carbons (PCs) by simply adjusting the elemental composition of their precursors with nitrogen-rich materials as additives. Nitrogen-modified enteromorpha prolifera–based (EP-based) PCs are prepared from EP and urea (or melamine). Overall, compared with the control PC without nitrogen modification, their pore structures and surface chemical properties present similar improvement. When used in supercapacitors, their specific capacitances increase by approximately 22% due to their significant development of mesopores at 2.5–7.0 nm, which increases the effective surface areas. With an appropriate amount of nitrogen-containing or oxygen-containing functional groups maintaining surface wettability, the notable increase of graphitized N improves their conductivity. Due to the higher graphitization degrees, their resistances are reduced. With more mesopores transporting ions, they exhibit excellent high-rate capacitive performance. Moreover, they show remarkable long cycle performance with the specific capacitance retention of larger than 92% after 10,000 cycles.

Keywords: enteromorpha prolifera, urea, melamine, porous carbon, pore structure, supercapacitor, electrochemical performance

OPEN ACCESS

Edited by:
Suresh Kannan Balasingam, Norwegian University of Science and Technology, Norway

Reviewed by:
Sathiyaraj Kandhasamy, Dutch Institute for Fundamental Energy Research, Netherlands
Ayyappan Elangovan, Kansas State University, United States

****Correspondence:***
Kuihua Han
hankh@163.com

Specialty section:
This article was submitted to Electrochemical Energy Conversion and Storage, a section of the journal Frontiers in Energy Research

Received: *15 February 2021*
Accepted: *10 May 2021*
Published: *28 May 2021*

Citation:
Li M, Han K, Teng Z, Wang M, Cao Y and Li X (2021) Preparation of High-Performance Enteromorpha Prolifera–Based Porous Carbons by Nitrogen Modification and Their Electrochemical Performance. Front. Energy Res. 9:668111. doi: 10.3389/fenrg.2021.668111

INTRODUCTION

Benefiting from the diversity of composition and structure of biomass, their derived PCs with developed pore structures have high potential as electrode materials for supercapacitors (Huang et al., 2017; Yang et al., 2019; Zhao et al., 2019; Khan et al., 2020; Qian et al., 2020; Liang et al., 2021). Generally, to prepare high-performance PCs from selected biomass, some measures are taken to optimize their microstructures during the preparation process (Xu et al., 2017; He et al., 2019; Li et al., 2020b; Lin et al., 2020; Luo et al., 2020; Sun et al., 2020; Wu et al., 2020a; Xie et al., 2020a). Although those previous measures can improve the electrochemical properties, they may also show some adverse effects. For example, element doping is an effective method to improve surface property due to the generated surface functional groups, but those functional groups may also cause structural instability, pore blockage, conductivity decline, and other problems; template-assisted methods can be used to optimize pore structures, but they may also show some shortcomings, such as impurity residue, complex synthesis process, limited application scope,

etc. Therefore, it is still necessary to further explore more advanced methods to fabricate high-quality PC products.

Nitrogen-rich materials are usually used as nitrogen sources for manufacturing N-doped PCs, but few studies are on their other potential applications (Chen et al., 2017; Zhang et al., 2019a; Li et al., 2020a; Song et al., 2020). By comparing the morphologies and pore structures of charcoals derived from alginic acid and ammonium alginate, our team found that nitrogen in ammonium alginate can promote a large number of thin-walled cavities in the carbonized sample, thus forming greatly developed pore structure in its derived PC. Although the mechanism of nitrogen regulation microstructure is still unclear, it is believed that nitrogen element in precursor can regulate the pore structure of its derived PC. In other words, it is possible to make the pore structure of the obtained PC better by adding nitrogen element into its precursor. Meaningfully, this provides a new application direction for nitrogen-rich substances in preparing PCs.

EP is a kind of natural wild green algae with strong natural reproduction ability. Although it is nontoxic, due to global climate change, water eutrophication, and other reasons, its large-scale growth destroys marine ecosystem (Smetacek and Zingone, 2013; Zhou et al., 2015; Sun et al., 2018; Zhang et al., 2019b; Zhang et al., 2021a). Typically, EP is used to produce low-cost agricultural fertilizers, and animal husbandry feeds, but this is not enough to achieve pollution control. For environmental protection and high-quality utilization of this biomass resource, researchers have tried to apply EP in pharmaceutical, chemical, environmental, and other industries (Chen et al., 2018; Li et al., 2018; Shao et al., 2019; Li et al., 2020c; Zhu et al., 2020; Zhang et al., 2021b). In recent years, PCs derived from EP for energy storage have attracted considerable attention. However, it still needs to improve their properties, such as pore structure, conductivity, surface properties, etc.

This study presents a facile and effective nitrogen modification strategy (NMS): add nitrogen-rich substances to biomass to change the elemental composition of precursors, and then improve the electrochemical performance of those prepared PCs by optimizing their pore structures and surface chemical properties. Use EP as raw material, urea or melamine as nitrogen-rich additive, and synthesize precursors by thoroughly mixing them. Then, PCs are prepared by activating carbonized samples, which are prepared by simply carbonizing precursors. Further, the morphologies, pore structures, and surface chemical properties of these samples are characterized, and their electrochemical properties are tested. The similarities and differences of the effects of the two different nitrogen-rich additives are analyzed by comparing the microstructures and electrochemical performance of the obtained PCs.

EXPERIMENTAL SECTIONS

Preparation of Nitrogen Modification Porous Carbons

After thoroughly washing with deionized water to remove impurities, EP (Ningbo, Zhejiang, China) was put into a drying oven and heated at 120°C until dry. Then it was pulverized into powder and screened with an 80-mesh sieve. Dry EP powder and urea (or melamine) (Sinopharm Chemical Reagent Co., Ltd., China) were mixed to get homogeneous precursor samples. The mass ratio of EP to urea (or melamine) was 5:1. The precursor composed of EP and urea as EPU-5, the precursor composed of EP and melamine were marked as EPM-5. Besides, EP was selected as the control precursor.

30 g precursor was placed in a horizontal tube furnace and heated to 600°C in a 1-L min^{-1} nitrogen stream, and then kept at this temperature for 2 h and cooled down to 80°C to obtain a carbonized product. The carbonized product was pickled with 5 mol L^{-1} HCl (Sinopharm Chemical Reagent Co., Ltd., China) and rinsed thoroughly with deionized water until neutral. Then it was heated at 105°C until dry to obtain a carbonized sample.

Then, based on previous studies by (Wang and Kaskel, 2012; Zhou et al., 2014; Gao et al., 2015; Lee et al., 2016; Li et al., 2017; Lin et al., 2018; Su et al., 2018), KOH was selected as the activator to develop pore structures, and optimized activation conditions were implemented. With a mass ratio of KOH to the carbonized sample of 4:1 and at 105°C, the carbonized sample was immersed in saturated KOH (Tianjin Kermel Chemical Reagent Co., Ltd., China) solution for 12 h. The mixture was placed in a muffle furnace and heated to 800°C in a 0.6-L min^{-1} nitrogen flow, and then kept at this temperature for 2 h and cooled down to 80°C to obtain an activation product. The activation product was pickled with 5 mol L^{-1} HCl and then rinsed thoroughly with deionized water until neutral. Then it was heated at 105°C until dry to obtain a PC sample. Throughout the experiment, a fixed heating rate of 5°C min^{-1} was used. The PC samples derived from EP, EPU-5, and EPM-5 were marked as EP-PC, EPU-PC-5, and EPM-PC-5, respectively. Besides, EP-PC was selected as the control PC.

Material Characterization

The morphologies of samples were observed by a SUPRA55 scanning electron microscope (SEM, Carl Zeiss AG, Germany). After 5 h of vacuum degassing at 300°C, their pore structures were analyzed with a JW-BK132F instrument (Beijing JWGB Sci&Tech Ltd., China) by nitrogen adsorption and desorption at 77.4 K. Their specific surface areas (S_{BET}s) were calculated by the Brunauer–Emmett–Teller (BET) method based on the nitrogen adsorption data within the P/P_0 range of 0.10 and 0.25. The amount of adsorbed nitrogen at P/P_0 = 0.993 was regarded as their total pore volumes (V_{total}s). Their micropore surface areas (S_{micro}s) and mesopore surface areas (S_{meso}s) were estimated by the t-plot method based on carbon black model. Their micropore volumes (V_{micro}s), average micropore sizes (D_{micro}s), and micropore size distributions were examined by the Horvath–Kawazoe (HK) method based on nitrogen adsorption data and a slit pore model. Their mesopore size distributions and average mesopore sizes (D_{meso}s) were obtained by the Barrett–Joyner–Halenda (BJH) method. Then their mesopore volumes (V_{meso}s) were calculated by the differences between V_{total}s and V_{micro}s. The states of C, N, and O elements in PCs were surveyed by X-ray photoelectron spectroscopy (XPS) with an ESCALAB 250XI (Thermo Fisher Scientific Inc., United States) instrument. Their surface chemical

FIGURE 1 | Synthesis mechanism of nitrogen-modified EP-based PC.

structures were analyzed by Raman spectroscopy with an RM 2000 (Renishaw Co., Ltd., United Kingdom) device and a 514-nm laser.

Electrochemical Characterization

Absolute ethyl alcohol (Sinopharm Chemical Reagent Co., Ltd., China) was used as the solvent, and then the homogeneous glue-like mixture of conducting graphite (TIMREX KS6), polytetrafluoroethylene (D210C, DAIKIN), and PC with a weight ratio of 1:1:8 was prepared. Then it was painted evenly on nickel foam pieces (300 g m^{-2}, about 1 mm thickness). Then these pieces were pressed at 12 MPa for 1 min, put into a vacuum, and kept at 80°C for 12 h to get dry electrode pieces.

PCs' electrochemical performance was measured with an electrochemical workstation (CS310H, Wuhan CorrTest Instruments Corp., Ltd., China) and a two-electrode system. A piece of separator paper (NKK-MPF30AC-100, Nippon Kodoshi Corporation), a pair of cell shells (2016-type), two electrode pieces (radius about 8 mm, thickness about 0.1 mm) with PC loads of about 4 mg, and KOH solution (6 mol L^{-1}) were assembled into a cell. These cell materials were purchased from Shanxi Cell Materials Co., Ltd., China.

Galvanostatic charge–discharge (GCD) tests were conducted with a current–density range of 0.1–50 A g^{-1}, and a potential window of 0–1 V. Cyclic voltammetry (CV) tests were conducted with a scan-rate range of 20–200 mV s^{-1}, and a potential window of 0–1 V. Electrochemical impedance spectroscopy (EIS) were measured with a frequency range of 10^{5}–10^{-3} Hz and an AC amplitude of 5 mV. Specific capacitance, discharge current, discharge time, the mass load of the PC in two electrode pieces, potential difference, energy density, and power density were marked as C, I, Δt, m, ΔV, E, and P, respectively. Then, the C of PC was calculated by **Eq. 1** based on the data from the discharge branch of GCD curve. And the E and P of a cell were estimated by **Eqs. 2**, **3**, respectively:

$$C = (4 * I * \Delta t) / (m * \Delta V), \quad (1)$$

$$E = C * (\Delta V)^2 / 8, \quad (2)$$

$$P = E/\Delta t. \quad (3)$$

RESULTS AND DISCUSSION

As shown in **Figure 1**, urea or melamine is added to EP to adjust the elemental composition of the precursor. During the carbonization process, EP and nitrogen-rich additive undergo complex physical and chemical reactions. Then due to the interaction of these reactions, the microstructures of the prepared carbonized sample are regulated. Afterward, its derived PC is improved accordingly in the microscopic morphologies, pore structures, and surface chemical properties and further shows excellent electrochemical properties. The carbonization reactions of urea and melamine are different, leading them to play different regulation effects on PCs. The details are as follows.

The SEM images of these prepared PCs are shown in **Figure 2**. EP-PC, EPU-PC-5, and EPM-PC-5 are, respectively, derived from EP, urea-modified EP, and melamine-modified EP, and they roughly present the structural characteristics of massive cracking, small carbon particle accumulation, and a large number of small slits, respectively. Then it can be concluded that NMS can effectively regulate the microstructure of the prepared PC, and the regulation effects of urea and melamine are different.

The nitrogen adsorption and desorption isotherm curves of EP-PC, EPU-PC-5, and EPM-PC-5 are shown in **Figure 3A**. When $P/P_0 < 0.4$, the trends of these three curves demonstrate that adsorption and filling occur in micropores (Yuan et al., 2021). And when $P/P_0 > 0.4$, the hysteresis loops on these curves demonstrate that capillary condensations occur in mesopores (Hamouda et al., 2021). Hence, all these PCs contain micropores and mesopores. However, the hysteresis loop corresponding to EP-PC is type H3, and those corresponding to EPU-PC-5 and EPM-PC-5 are type H4, indicating that NMS can change the pore architecture of PCs.

Based on the data from **Table 1**, calculations show that the S_{BET}s of EPU-PC-5 and EPM-PC-5 are 0.98 and 1.01 times that of EP-PC, respectively, indicating that the S_{BET}s of these three PCs are almost equal. The V_{total}s of EPU-PC-5 and EPM-PC-5 are 1.19 and 1.15 times that of EP-PC, respectively, while the V_{micro}s of these three are similar, suggesting that the increase of V_{total}s is mainly caused by the increase of V_{meso}s. Furthermore, these three PCs have equal D_{micro}s, while the relationship of their D_{meso}s is EPU-PC-5 > EPM-PC-5 > EP-PC. Therefore, it can be concluded that the effects of urea or melamine modification on pore structures are generally similar: they have little effects on micropore structures but can significantly promote the development of mesopore structures with almost no change in S_{BET}s. Besides, in comparison, urea modification in promoting the development of mesopores is slightly better than that of melamine modification.

The micropore size distributions of EP-PC, EPU-PC-5, and EPM-PC-5 are shown in **Figure 3B**. The trends of these three curves are similar, and micropores are mainly distributed in the range of below 0.80 nm with almost the same positions of the extreme points on each curve. In the range of below 0.59 nm, the relationship of the extreme values corresponding to the same extreme point is roughly EPM-PC-5 > EP-PC > EPU-PC-5. However, in the range of 0.59–2.00 nm, the extreme values

FIGURE 2 | SEM images of EP-PC **(A)**, EPU-PC-5 **(B)**, and EPM-PC-5 **(C)**.

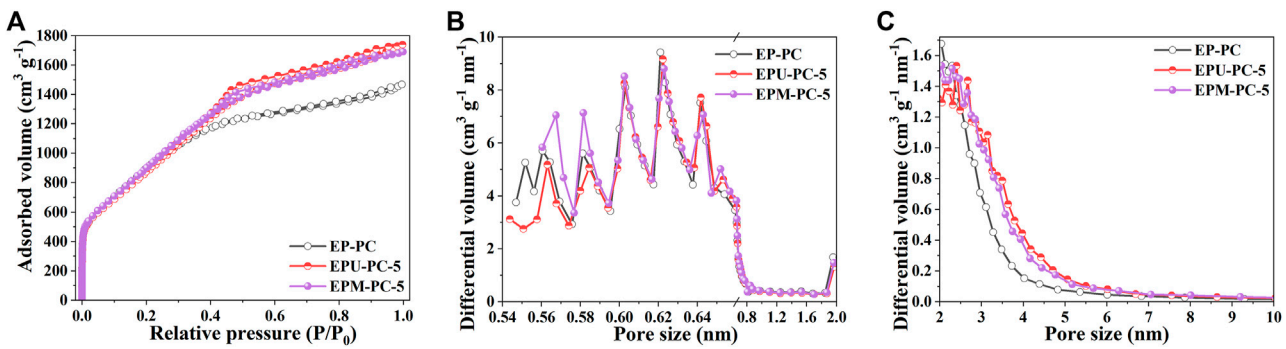

FIGURE 3 | Pore structure analysis of EP-PC, EPU-PC-5, and EPM-PC-5. **(A)** N_2 adsorption and desorption isotherm curves. **(B)** Micropore size distributions. **(C)** Mesopore size distributions.

TABLE 1 | Pore structure parameters of EP-PC, EPU-PC-5, and EPM-PC-5.

sample	S_{BET}[a]	V_{total}[b]	D_{micro}[c]	D_{meso}[d]	S_{meso}[e]/S_{micro}[f]	V_{micro}/V_{total}
	m^2g^{-1}	cm^3g^{-1}	nm	nm		
EP-PC	3,505.7	2.27	0.66	2.99	0.28	0.52
EPU-PC-5	3,427.1	2.69	0.66	3.26	0.53	0.43
EPM-PC-5	3,556.6	2.62	0.66	3.14	0.48	0.46

[a]*Specific surface area.*
[b]*Total pore volume.*
[c]*Average micropore size.*
[d]*Average mesopore size.*
[e]*Mesopore surface area.*
[f]*Micropore surface area.*

corresponding to the same extreme point are almost equal. Thus, the variation of these micropore size distributions can suggest that NMS has little effect on micropore size distributions, but only has a particular effect on the distributions of smaller pores (<0.59 nm). Their mesopore size distributions are shown in **Figure 3C**. On the whole, the trends of these curves are similar, and mesopores are mainly distributed in the range of 2.0–7.0 nm, but they differ in the range of 2.0–3.0 nm. Besides, it is observed that in the range of 2.5–7.0 nm, EPU-PC-5 has more mesopores than EPM-PC-5 and EPM-PC-5 has more mesopores than EP-PC, which also demonstrates that NMS can promote the development of mesopores, and those increased mesopores are primarily located in the range of 2.5–7.0 nm.

The Raman spectra of EP-PC, EPU-PC-5, and EPM-PC-5 are shown in **Figure 4**. The D bands located around 1,349 cm^{-1} of them are considered as the disordered vibration peaks caused by structural defects, their G bands located around 1,590 cm^{-1} are caused by the vibration of sp^2 C, and the 2D bands located around 2,871 cm^{-1} mean that these PCs have good atomic order (Teng et al., 2020; Nguyen et al., 2021). The relative intensity ratios of G band to D band (I_G/I_D) can indicate their degrees of graphitization. Accordingly, the relationship of graphitization degree of

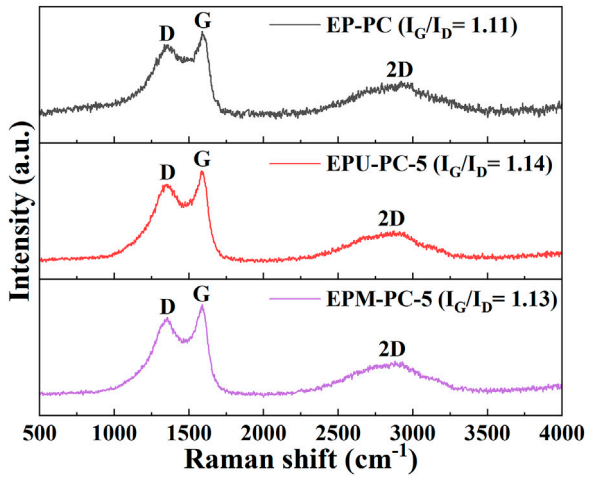

FIGURE 4 | Raman spectra of EP-PC, EPU-PC-5, and EPM-PC-5.

them is EPU-PC-5 > EPM-PC-5 > EP-PC. However, their values of I_G/I_D are very close, suggesting that NMS can slightly improve graphitization degree, and the effect of urea is relatively better than that of melamine.

The XPS spectra of EP-PC, EPU-PC-5, and EPM-PC-5 are shown in **Figure 5**. All these three PCs have C, N, and O elements (**Figures 5A–C**). Furthermore, the data from **Table 2** shows that the contents of each element in EPU-PC-5 and EPM-PC-5 are almost equal, and they have more C and less N and O than EP-PC, indicating that both of urea and melamine modification can increase the content of C and reduce the contents of N and O. More C may mean stronger conductivity, and less N and O may mean weaker surface wettability. Their C1s spectra can be deconvoluted into four separate peaks (**Figures 5D–F**). The relative intensity contents of each peak for these three PCs are similar (**Table 2**), indicating that NMS hardly change the existing state of C element. Besides, the relative intensity ratios of C=C and C–C are larger than those of the others, implying that these three PCs have good conductivity. The N1s spectra can be deconvoluted into four separate peaks (**Figures 5G–I**). EP-PC has more pyridine N and pyrrole N, the relative intensity ratios of these four peaks of EPU-PC-5 are all above 20%, and EPM-PC-5 has more pyrrole N and graphitized N (**Table 2**). Generally, it is considered that pyridine N and pyrrole N are helpful to improve surface wettability, and graphitized N can enhance conductivity, and oxidized N is similar to nitrogen–oxygen functional groups (Lin et al., 2018; Wu et al., 2019). Thus, it can be concluded that NMS can significantly increase graphitized N and reduce pyridine N. Besides, it is noticed that the existing states of N element in EPU-PC-5 and EPM-PC-5 are different. The O1s spectra can be deconvoluted into four separate peaks (**Figures 5J–L**). All these PCs have more C=O and C-OH and C-O-C than others (**Table 2**), which helps to enhance surface wettability (Lin et al., 2021). Then, it is concluded that both urea and melamine modifications can increase the contents of C element, and the content of each element in these two PCs is similar, but their existing states differ a lot, especially N element.

Further, the electrochemical performance of these obtained PCs is tested on a two-electrode system. The CV curves of EP-PC, EPU-PC-5, and EPM-PC-5 are shown in **Figures 6A–C**. The rectangular CV curves corresponding to these three PCs indicate that the tested cells present good electric double-layer behaviors, implying that the pseudocapacitances can be ignored. And it is observed that when the scan rate changes from 20 – 200 mV s^{-1}, the relationship of the rectangular shape distortions of these CV curves is EPU-PC-5 > EP-PC > EPM-PC-5, meaning that the relationship of their charge transfer capacities is EPU-PC-5 < EP-PC < EPM-PC-5. Compared with EP-PC, the charge transfer capacity of EPU-PC-5 decreases, which is because although the more mesopores of EPU-PC-5 are beneficial to improve its charge transfer capacity, the weakened effects caused by the decrease of N, O, pyridine N, and pyrrole N are stronger; and the charge transfer capacity of EPM-PC-5 increases, which is because limited by the pore structure, although EP-PC has more surface functional groups, they only have a small effect on improving the charge transfer capacity, while the more mesopores of EPM-PC-5 improve its charge transfer capacity greatly. Besides, it is noticed that although both of EPU-PC-5 and EPM-PC-5 have more mesopores, the effects of those mesopores on improving their charge transfer capacity are different, which may be caused by the different three-dimensional structures of their pores (**Figure 2**). These results indicate that NMS can affect charge transfer capacity through regulating pore structures and surface properties.

The GCD curves corresponding to these three PCs are typical performance curves of electric double-layer capacitors (**Figures 6D–F**). According to **Eq. (1)**, it is calculated that when the current density is 0.1, 0.2, 0.5, 1.0, and 2.0 A g^{-1}, the specific capacitances of EP-PC are 278.3, 264.9, 252.3, 244.7, and 236.2 F g^{-1}, respectively, and those of EPU-PC-5 are 344.6, 323.9, 308.0, 297.8, and 286.9 F g^{-1}, respectively, and those of EPM-PC-5 are 352.9, 334.3, 315.0, 305.8, and 296.5 F g^{-1}, respectively. Compared with those reported EP-based PCs, the specific capacitances of EPU-PC-5 and EPM-PC-5 are significantly larger (Gao et al., 2014a; Gao et al., 2014b; Gai et al., 2015; Tian et al., 2016; Ren et al., 2018; Xie et al., 2020b). Further calculations indicate that under the same current density, the specific capacitance of EPU-PC-5 is approximately 1.22 times that of EP-PC, and the specific capacitance of EPM-PC-5 is approximately 1.26 times that of EP-PC. It is noticed that the S_{BET}s of EP-PC are similar to those of the other two PCs (**Table 1**), and it has more N and O (**Table 2**), whose corresponding functional groups can provide pseudocapacitance. Still, its specific capacitance is significantly lower than that of the other two. For these tested cells, the surfaces in PCs that can provide capacitance are effective, and those surfaces which ions cannot access are ineffective. Thus, it can be inferred that the effective S_{BET}s of EP-PC are markedly smaller than the other two. That is to say, the increase in specific capacitances of EPU-PC-5 and EPM-PC-5 is mainly due to the development of their mesopore structures which can increase their effective S_{BET}s.

According to **Eqs. 2**, **3**, the energy densities and power densities of these three PC-based cells are, respectively,

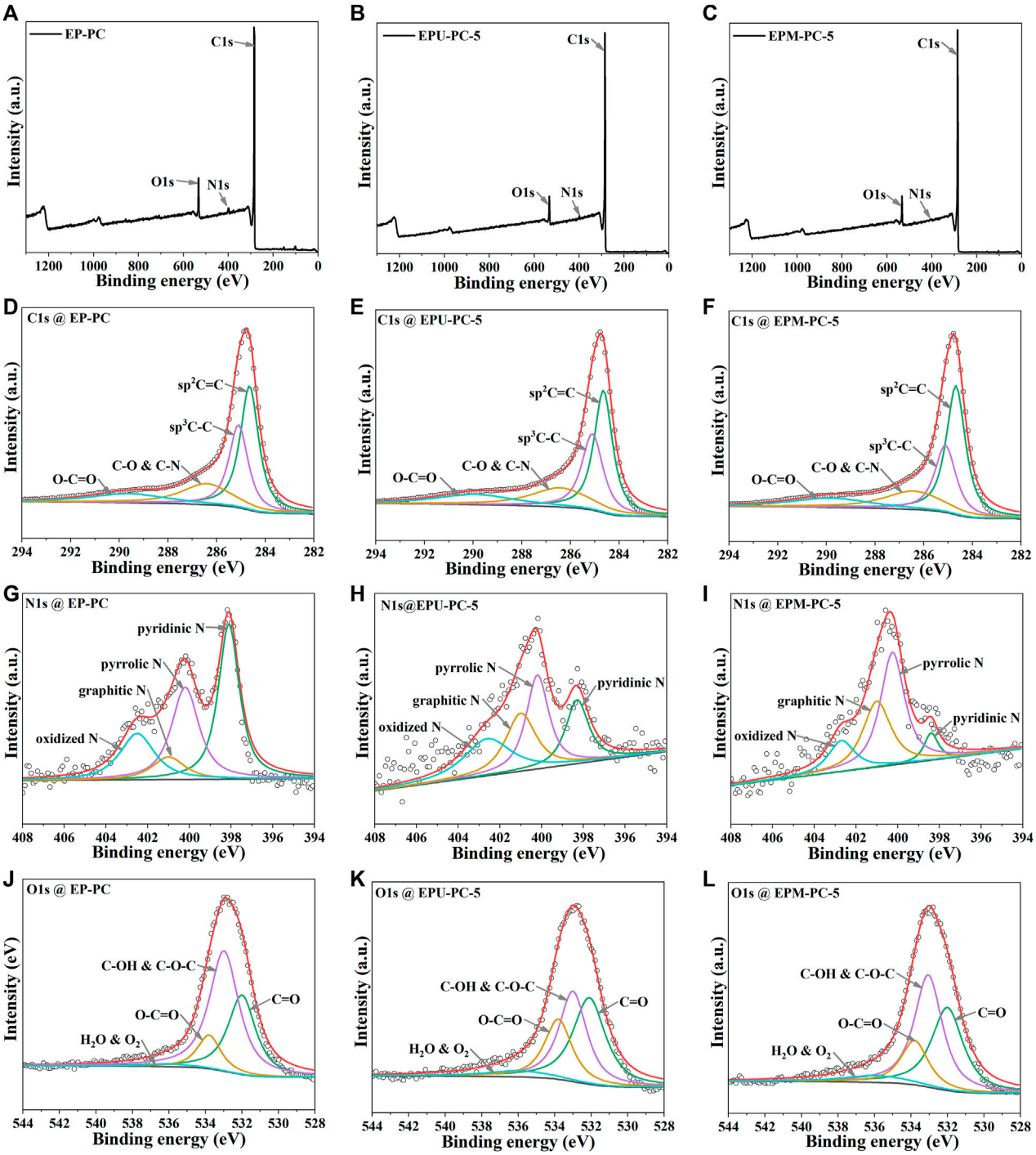

FIGURE 5 | XPS analysis of EP-PC, EPU-PC-5, and EPM-PC-5. **(A–C)** XPS survey. **(D–F)** C1s. **(G–I)** N1s. **(J–L)** O1s.

calculated, and the results are shown in **Figure 7A**. EP-PC–based cell has an energy density of 9.7 Wh kg^{-1} with a power density of 49.9 W kg^{-1}, EPU-PC-5–based cell has an energy density of 11.9 Wh kg^{-1} with a power density of 49.7 W kg^{-1}, and EPM-PC-5–based cell has an energy density of 12.2 Wh kg^{-1} with a power density of 46.0 W kg^{-1}. Besides, it can be observed that under the same power density, the energy densities of EPU-PC-5– and EPM-PC-5–based cells are larger than that of EP-PC–based cell, indicating that NMS can improve the energy storage performance of the PC corresponding devices.

The rate performance curves of EP-PC, EPU-PC-5, and EPM-PC-5 in **Figure 7B** present similar trends. Their specific

TABLE 2 | XPS analysis of surface chemical compositions of EP-PC, EPU-PC-5, and EPM-PC-5.

peak	Chemical state	Binding energy	EP-PC		EPU-PC-5		EPM-PC-5	
		eV	RIR[a]	ER[b]	RIR[a]	ER[b]	RIR[a]	ER[b]
			%					
C1s	sp^2 C=C	284.7	40.7	89.78	38.7	92.51	43.0	92.34
	sp^3 C-C	285.1	28.0		27.7		24.8	
	C-O and C-N	286.4	18.8		19.5		19.1	
	O-C=O	289.8	12.5		14.1		13.1	
N1s	pyridine N	398.3	40.2	2.22	20.7	0.84	6.6	0.85
	pyrrole N	400.2	31.0		30.0		47.3	
	graphitized N	401.0	9.1		24.8		32.0	
	oxidized N	402.6	19.7		24.5		14.1	
O1s	C=O	532.1	33.0	8.00	38.2	6.65	35.2	6.81
	C-OH and C-O-C	533.0	53.2		34.0		42.3	
	O-C=O	533.8	11.8		22.3		16.4	
	H_2O and O_2	535.9	2.0		5.5		6.1	

[a]*Relative intensity ratio.*
[b]*Elemental ratio.*

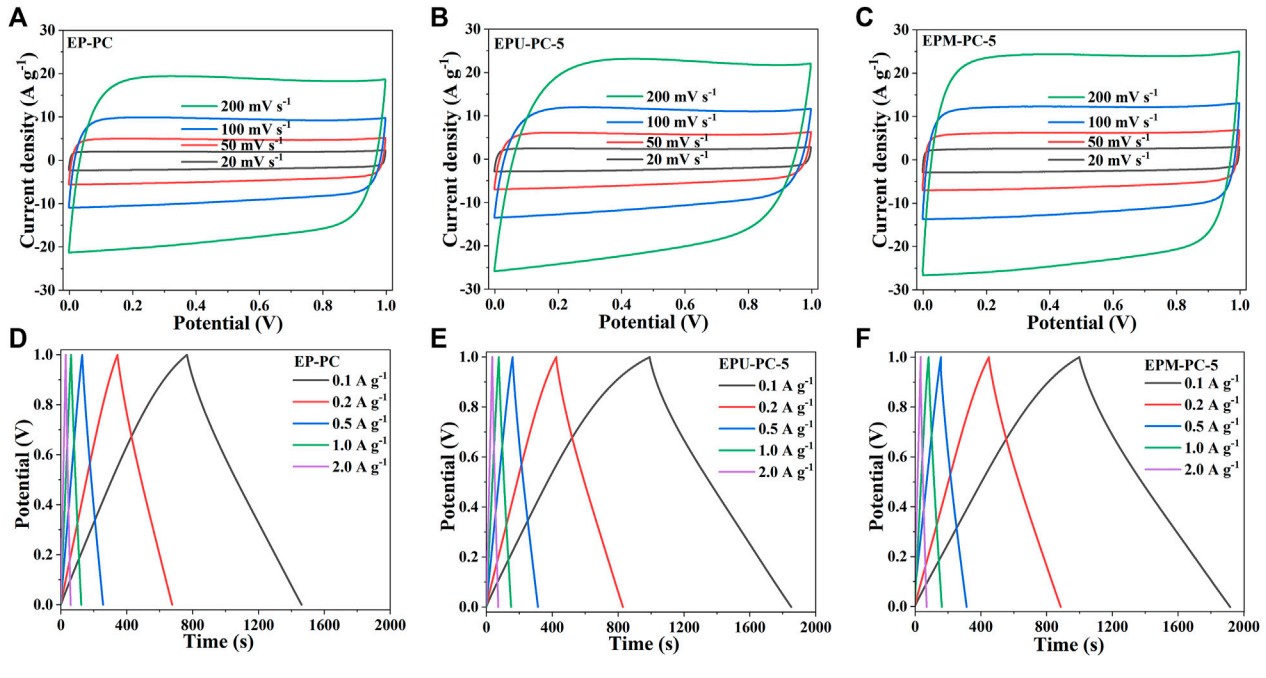

FIGURE 6 | CV **(A–C)** and GCD **(D–F)** curves of EP-PC, EPU-PC-5, and EPM-PC-5.

capacitances decrease as current densities increase, which is mainly caused by the increase of electrode concentration polarization due to the slow diffusion of ions, which increases the internal resistance (Zhang et al., 2018; Mehare et al., 2020). It is observed that when less than 2 A g^{-1}, their specific capacitances show rapid decay, and when larger than 2 A g^{-1}, their specific capacitances show slow decay. Furthermore, when less than 30 A g^{-1}, the decay rates of these three curves are similar, and when larger than 30 A g^{-1}, the relationship of their decay rates is EP-PC > EPM-PC-5 > EPU-PC-5, indicating that the relationship of their rate performance is EP-PC < EPM-PC-5 < EPU-PC-5. The better rate performance of EPU-PC-5 and EPM-PC-5 should be mainly due to their more developed mesopore structures.

The Nyquist plots of EP-PC, EPU-PC-5, and EPM-PC-5 are shown in **Figure 8A**. In low-frequency range, these three curves are nearly vertical, indicating that their corresponding cells present idealized electric double-layer behaviors. In the high-frequency range, the diameter of the semicircular arc in the curve usually represents the charge-transfer resistance related to Faradic reactions between ions and oxygen-containing or nitrogen-containing functional groups on electrode material,

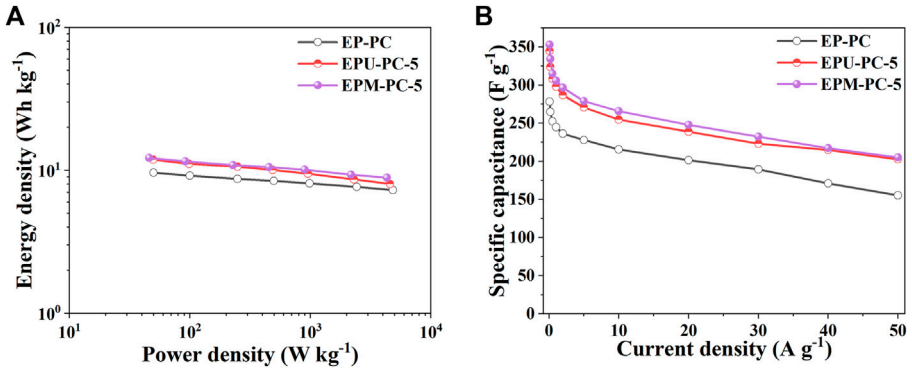

FIGURE 7 | (A) Ragone plots and **(B)** rate performance curves for EP-PC, EPU-PC-5, and EPM-PC-5.

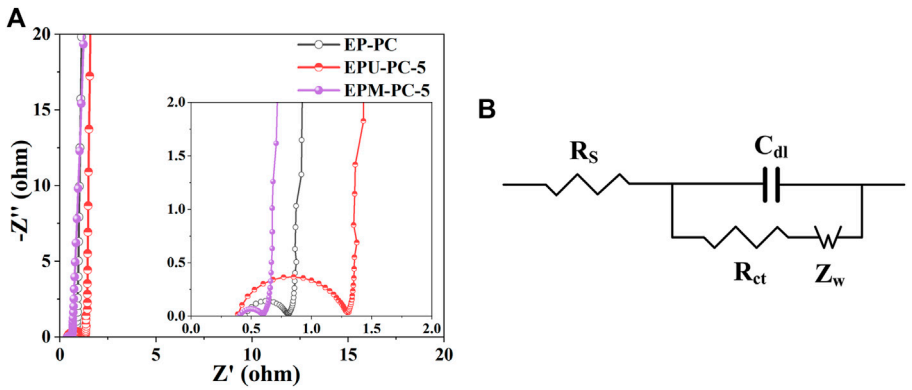

FIGURE 8 | (A) Nyquist plots for EP-PC, EPU-PC-5, and EPM-PC-5, and **(B)** equivalent circuit diagram for those tested supercapacitors.

which corresponds to R_{ct} in **Figure 8B** (Song et al., 2015). Therefore, as shown in **Supplementary Table S1**, the relationship of the charge-transfer resistances of cells corresponding to these three PCs is EPU-PC-5 (0.85 Ω) > EP-PC (0.32 Ω) > EPM-PC-5 (0.17 Ω). Evidently, large charge-transfer resistance means weak charge-transfer capacity. Therefore, the above result is consistent with the relationship of the charge-transfer capacity reflected by those CV curves (**Figures 6D–F**). The intercepts on the Z' axis represent the equivalent-series resistances (ESRs) related to the intrinsic resistances of electrode materials and electrolyte, and the contact resistance between working and reference electrodes, which corresponds to R_s in **Figure 8B** (Yu et al., 2017; Zhu et al., 2017). Thus, as shown in **Supplementary Table S1**, the relationship of the ESRs of the cells corresponding to PCs is EP-PC (0.45 Ω) > EPM-PC-5 (0.40 Ω) > EPU-PC-5 (0.38 Ω). Then it is concluded that NMS can reduce the ESRs of those cells, which is mainly attributed to the enhancement of the conductivities of those nitrogen modified PCs with the improvement of graphitization degrees.

The cycle performance curves of EP-PC, EPU-PC-5, and EPM-PC-5 in **Figure 9** obtained at 5 A g^{-1} for 10,000 cycles show similar three stages, and the comparison diagrams of GCD curves corresponding to the first and 10000th cycles are shown in **Supplementary Figure S1**. Each stage in each curve has almost equal retention of specific capacitance, suggesting that highly reversible double-layer behaviors occur at electrodes. As curves go from stage 1 to stage 2 and then to stage 3, the specific capacitance retentions suddenly increase and then suddenly decrease. These changes may be due to ion desolvation occurring, which allows ions to enter micropores to generate capacitance (Urita et al., 2014; Wu et al., 2020b), and then micropores are filled with ions and no capacitance is generated. Besides, all their specific capacitance retentions are larger than 92.0%, indicating that the cells corresponding to these nitrogen modified EP-based PCs can maintain excellent long-cycle performance.

CONCLUSION

In summary, NMS can improve the electrochemical performance of PCs by optimizing their pore structures and surface chemical properties. Urea and melamine are used as nitrogen-rich additives to prepare nitrogen-modified EP-based PCs through carbonization and activation. On the one hand, the two nitrogen-

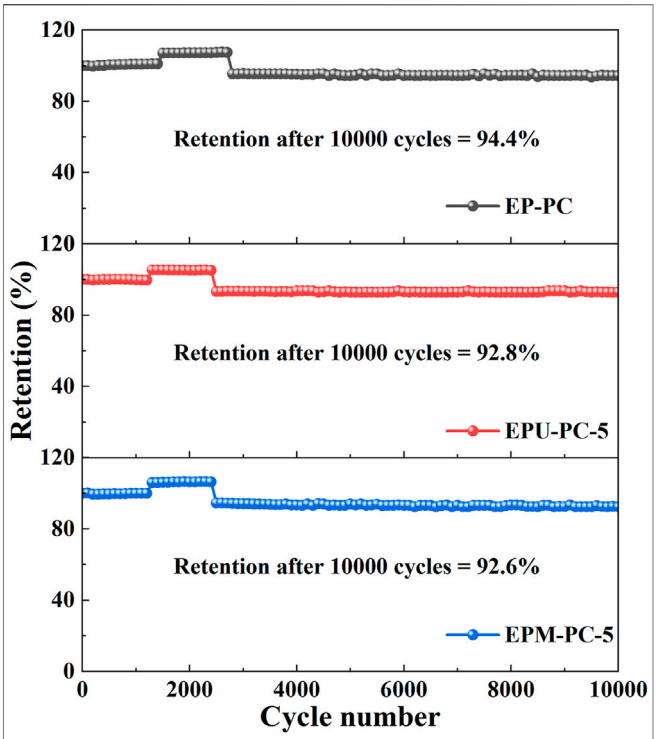

FIGURE 9 | Cycle performance curves of EP-PC, EPU-PC-5, and EPM-PC-5.

rich additives can promote the development of the mesoporous structures of the obtained PCs and can improve their graphitization degrees with almost unchanged S_{BET}s. The effect of urea is slightly better than that of melamine. On the other hand, both of them can increase the contents of C element in PCs and can greatly increase the relative intensity contents of graphitized N. It is noticed that the content of each element in those two nitrogen modified EP-based PCs is almost equal, but the existing state of each element is different, especially N element. Benefiting from the optimized microstructures, the specific capacitances of nitrogen modified EP-based PCs are increased by approximately 22%, their high-rate performance is enhanced, the ESRs of their corresponding cells are reduced, and they show excellent long-cycle performance. Considering the simple process and remarkable effect of NMS, it offers great potential to apply in the preparation of PCs, and it can combine with other postprocessing methods to further improve the performance of PCs.

DATA AVAILABILITY STATEMENT

The original contributions presented in the study are included in the article/**Supplementary Material**, further inquiries can be directed to the corresponding author.

AUTHOR CONTRIBUTIONS

ML conducted the experiments and scientific discussions. KH contributed to research suggestions. ZT helped with writing. MW helped with characterization. YC and XL helped with experiments. All authors listed made a substantial and intellectual contribution to the work and approved it for publication.

FUNDING

This work was supported by the Natural Science Foundation of Shandong, China (ZR2017MEE010), and the Fundamental Research Funds of Shandong University (2016JC005).

SUPPLEMENTARY MATERIAL

The Supplementary Material for this article can be found online at: https://www.frontiersin.org/articles/10.3389/fenrg.2021.668111/full#supplementary-material

REFERENCES

Chen, Y., Wang, B., Xin, J., Sun, P., and Wu, D. (2018). Adsorption Behavior and Mechanism of Cr(VI) by Modified Biochar Derived from Enteromorpha Prolifera. *Ecotoxicology Environ. Saf.* 164, 440–447. doi:10.1016/j.ecoenv.2018.08.024

Chen, Z., Peng, X., Zhang, X., Jing, S., Zhong, L., and Sun, R. (2017). Facile Synthesis of Cellulose-Based Carbon with Tunable N Content for Potential Supercapacitor Application. *Carbohydr. Polym.* 170, 107–116. doi:10.1016/j.carbpol.2017.04.063

Gai, Y., Wang, L., Gong, L., Su, L., Shang, Y., Dong, F., et al. (2015). Ultrafast Microwave Synthesis of Activated Carbon from Enteromorpha Prolifera and its Electrochemical Capacitive Behavior. *Chem. Lett.* 44 (11), 1613–1615. doi:10.1246/cl.150703

Gao, X., Xing, W., Zhou, J., Wang, G., Zhuo, S., Liu, Z., et al. (2014a). Superior Capacitive Performance of Active Carbons Derived from Enteromorpha Prolifera. *Electrochimica Acta* 133, 459–466. doi:10.1016/j.electacta.2014.04.101

Gao, Y., Li, L., Jin, Y., Wang, Y., Yuan, C., Wei, Y., et al. (2015). Porous Carbon Made from rice Husk as Electrode Material for Electrochemical Double Layer Capacitor. *Appl. Energ.* 153, 41–47. doi:10.1016/j.apenergy.2014.12.070

Gao, Y., Zhang, W., Yue, Q., Gao, B., Sun, Y., Kong, J., et al. (2014b). Simple Synthesis of Hierarchical Porous Carbon from Enteromorpha Prolifera by a Self-Template Method for Supercapacitor Electrodes. *J. Power Sourc.* 270, 403–410. doi:10.1016/j.jpowsour.2014.07.115

Hamouda, H. A., Cui, S., Dai, X., Xiao, L., Xie, X., Peng, H., et al. (2021). Synthesis of Porous Carbon Material Based on Biomass Derived from hibiscus Sabdariffa Fruits as Active Electrodes for High-Performance Symmetric Supercapacitors. *RSC Adv.* 11 (1), 354–363. doi:10.1039/d0ra09509e

He, D., Zhao, W., Li, P., Sun, S., Tan, Q., Han, K., et al. (2019). Bifunctional Biomass-Derived N, S Dual-Doped Ladder-like Porous Carbon for Supercapacitor and Oxygen Reduction Reaction. *J. Alloys Comp.* 773, 11–20. doi:10.1016/j.jallcom.2018.09.141

Huang, Y., He, J., Luan, Y., Jiang, Y., Guo, S., Zhang, X., et al. (2017). Promising Biomass-Derived Hierarchical Porous Carbon Material for High Performance Supercapacitor. *RSC Adv.* 7 (17), 10385–10390. doi:10.1039/c6ra27788h

Khan, A., Senthil, R. A., Pan, J., Osman, S., Sun, Y., and Shu, X. (2020). A New Biomass Derived Rod-like Porous Carbon from tea-waste as Inexpensive and Sustainable Energy Material for Advanced Supercapacitor Application. *Electrochimica Acta* 335, 135588. doi:10.1016/j.electacta.2019.135588

Lee, J.-S. M., Briggs, M. E., Hasell, T., and Cooper, A. I. (2016). Hyperporous Carbons from Hypercrosslinked Polymers. *Adv. Mater.* 28 (44), 9804–9810. doi:10.1002/adma.201603051

Li, J., Han, K., Wang, D., Teng, Z., Cao, Y., Qi, J., et al. (2020a). Fabrication of High Performance Structural N-Doped Hierarchical Porous Carbon for Supercapacitors. *Carbon* 164, 42–50. doi:10.1016/j.carbon.2020.03.044

Li, J., Jiang, F., Chi, Z., Han, D., Yu, L., and Liu, C. (2018). Development of Enteromorpha Prolifera Polysaccharide-Based Nanoparticles for Delivery of Curcumin to Cancer Cells. *Int. J. Biol. Macromolecules* 112, 413–421. doi:10.1016/j.ijbiomac.2018.02.002

Li, M., Han, K., Gao, Y., Teng, Z., Li, J., and Wang, M. (2020b). Calcium-assisted Regulation of the Structures of Porous Carbons at the Micro-nano Scale. *J. Nanoelectronics Optoelectronics* 15 (2), 284–290. doi:10.1166/jno.2020.2700

Li, S., Han, K., Li, J., Li, M., and Lu, C. (2017). Preparation and Characterization of Super Activated Carbon Produced from Gulfweed by KOH Activation. *Microporous Mesoporous Mater.* 243, 291–300. doi:10.1016/j.micromeso.2017.02.052

Li, X., Wang, C., Tian, J., Liu, J., and Chen, G. (2020c). Comparison of Adsorption Properties for Cadmium Removal from Aqueous Solution by Enteromorpha Prolifera Biochar Modified with Different Chemical Reagents. *Environ. Res.* 186, 109502. doi:10.1016/j.envres.2020.109502

Liang, X., Liu, R., and Wu, X. (2021). Biomass Waste Derived Functionalized Hierarchical Porous Carbon with High Gravimetric and Volumetric Capacitances for Supercapacitors. *Microporous Mesoporous Mater.* 310, 110659. doi:10.1016/j.micromeso.2020.110659

Lin, G., Ma, R., Zhou, Y., Liu, Q., Dong, X., and Wang, J. (2018). KOH Activation of Biomass-Derived Nitrogen-Doped Carbons for Supercapacitor and Electrocatalytic Oxygen Reduction. *Electrochimica Acta* 261, 49–57. doi:10.1016/j.electacta.2017.12.107

Lin, G., Wang, Q., Yang, X., Cai, Z., Xiong, Y., and Huang, B. (2020). Preparation of Phosphorus-Doped Porous Carbon for High Performance Supercapacitors by One-step Carbonization. *RSC Adv.* 10 (30), 17768–17776. doi:10.1039/d0ra02398a

Lin, L., Lei, Y., Xie, H., Ou, J., and Liu, X. (2021). A Multifunctional Activation Strategy of Ultrathin Carbon Layers-Intertwined Carbon Microspheres Clusters towards Markedly Enhanced Capacitance. *J. Porous Mater.* 28 (2), 567–578. doi:10.1007/s10934-020-01009-5

Luo, L., Zhou, Y., Yan, W., Wu, X., Wang, S., and Zhao, W. (2020). Two-step Synthesis of B and N Co-doped Porous Carbon Composites by Microwave-Assisted Hydrothermal and Pyrolysis Process for Supercapacitor Application. *Electrochimica Acta* 360, 137010. doi:10.1016/j.electacta.2020.137010

Mehare, M. D., Deshmukh, A. D., and Dhoble, S. J. (2020). Preparation of Porous Agro-Waste-Derived Carbon from Onion Peel for Supercapacitor Application. *J. Mater. Sci.* 55 (10), 4213–4224. doi:10.1007/s10853-019-04236-7

Nguyen, N. T., Le, P. A., and Phung, V. B. T. (2021). Biomass-derived Carbon hooks on Ni Foam with Free Binder for High Performance Supercapacitor Electrode. *Chem. Eng. Sci.* 229, 116053. doi:10.1016/j.ces.2020.116053

Qian, L., Guo, F., Jia, X., Zhan, Y., Zhou, H., Jiang, X., et al. (2020). Recent Development in the Synthesis of Agricultural and Forestry Biomass-Derived Porous Carbons for Supercapacitor Applications: a Review. *Ionics* 26 (8), 3705–3723. doi:10.1007/s11581-020-03626-1

Ren, M., Jia, Z., Tian, Z., Lopez, D., Cai, J., Titirici, M. M., et al. (2018). High Performance N-Doped Carbon Electrodes Obtained via Hydrothermal Carbonization of Macroalgae for Supercapacitor Applications. *Chemelectrochem* 5 (18), 2686–2693. doi:10.1002/celc.201800603

Shao, W., Zhang, H., Duan, R., Xie, Q., Hong, Z., and Xiao, Z. (2019). A Rapid and Scalable Integrated Membrane Separation Process for Purification of Polysaccharides from Enteromorpha Prolifera. *Nat. Product. Res.* 33 (21), 3109–3119. doi:10.1080/14786419.2018.1519823

Smetacek, V., and Zingone, A. (2013). Green and golden Seaweed Tides on the Rise. *Nature* 504 (7478), 84–88. doi:10.1038/nature12860

Song, S., Ma, F., Wu, G., Ma, D., Geng, W., and Wan, J. (2015). Facile Self-Templating Large Scale Preparation of Biomass-Derived 3D Hierarchical Porous Carbon for Advanced Supercapacitors. *J. Mater. Chem. A.* 3 (35), 18154–18162. doi:10.1039/c5ta04721h

Song, Y., Qu, W., He, Y., Yang, H., Du, M., Wang, A., et al. (2020). Synthesis and Processing Optimization of N-Doped Hierarchical Porous Carbon Derived from Corncob for High Performance Supercapacitors. *J. Energ. Storage* 32, 101877. doi:10.1016/j.est.2020.101877

Su, X.-L., Chen, J.-R., Zheng, G.-P., Yang, J.-H., Guan, X.-X., Liu, P., et al. (2018). Three-dimensional Porous Activated Carbon Derived from Loofah Sponge Biomass for Supercapacitor Applications. *Appl. Surf. Sci.* 436, 327–336. doi:10.1016/j.apsusc.2017.11.249

Sun, S., Han, F., Wu, X., and Fan, Z. (2020). One-step Synthesis of Biomass Derived O, N-Codoped Hierarchical Porous Carbon with High Surface Area for Supercapacitors. *Chin. Chem. Lett.* 31 (9), 2235–2238. doi:10.1016/j.cclet.2019.11.023

Sun, X., Wu, M., Xing, Q., Song, X., Zhao, D., Han, Q., et al. (2018). Spatio-temporal Patterns of Ulva Prolifera Blooms and the Corresponding Influence on Chlorophyll-A Concentration in the Southern Yellow Sea, China. *Sci. Total Environ.* 640-641, 807–820. doi:10.1016/j.scitotenv.2018.05.378

Teng, Z., Han, K., Li, J., Gao, Y., Li, M., and Ji, T. (2020). Ultrasonic-assisted Preparation and Characterization of Hierarchical Porous Carbon Derived from Garlic Peel for High-Performance Supercapacitors. *Ultrason. Sonochem.* 60, 104756. doi:10.1016/j.ultsonch.2019.104756

Tian, Z., Xiang, M., Zhou, J., Hu, L., and Cai, J. (2016). Nitrogen and Oxygen-Doped Hierarchical Porous Carbons from Algae Biomass: Direct Carbonization and Excellent Electrochemical Properties. *Electrochimica Acta* 211, 225–233. doi:10.1016/j.electacta.2016.06.053

Urita, K., Ide, N., Isobe, K., Furukawa, H., and Moriguchi, I. (2014). Enhanced Electric Double-Layer Capacitance by Desolvation of Lithium Ions in Confined Nanospaces of Microporous Carbon. *Acs Nano* 8 (4), 3614–3619. doi:10.1021/nn500169k

Wang, J., and Kaskel, S. (2012). KOH Activation of Carbon-Based Materials for Energy Storage. *J. Mater. Chem.* 22 (45), 23710–23725. doi:10.1039/c2jm34066f

Wu, F., Gao, J., Zhai, X., Xie, M., Sun, Y., Kang, H., et al. (2019). Hierarchical Porous Carbon Microrods Derived from Albizia Flowers for High Performance Supercapacitors. *Carbon* 147, 242–251. doi:10.1016/j.carbon.2019.02.072

Wu, J.-C., Liu, C., Zhou, H., Liu, M., Zhang, D., Yu, C., et al. (2020b). Thermal Dynamic Study of the Gradual Desolvation in Submicropores for Carbon-Based Supercapacitor at Low Temperature. *Ionics* 26 (9), 4695–4704. doi:10.1007/s11581-020-03575-9

Wu, J., Xia, M., Zhang, X., Chen, Y., Sun, F., Wang, X., et al. (2020a). Hierarchical Porous Carbon Derived from wood Tar Using Crab as the Template: Performance on Supercapacitor. *J. Power Sourc.* 455, 227982. doi:10.1016/j.jpowsour.2020.227982

Xie, L., Jin, Z., Dai, Z., Chang, Y., Jiang, X., and Wang, H. (2020a). Porous Carbons Synthesized by Templating Approach from Fluid Precursors and Their Applications in Environment and Energy Storage: A Review. *Carbon* 170, 100–118. doi:10.1016/j.carbon.2020.07.034

Xie, T., Wang, J., Liu, X., Shang, Y., Ma, C., Su, L., et al. (2020b). Hierarchical Porous Activated Carbon Derived from Enteromorpha Prolifera for superior Electrochemical Capacitive Behavior. *Ionics* 26 (1), 403–413. doi:10.1007/s11581-019-03223-x

Xu, J., Zhang, W., Hou, D., Huang, W., and Lin, H. (2017). Hierarchical Porous Carbon Derived from Allium Cepa for Supercapacitors through Direct Carbonization Method with the Assist of Calcium Acetate. *Chin. Chem. Lett.* 28 (12), 2295–2297. doi:10.1016/j.cclet.2017.10.041

Yang, H., Ye, S., Zhou, J., and Liang, T. (2019). Biomass-derived Porous Carbon Materials for Supercapacitor. *Front. Chem.* 7, 274. doi:10.3389/fchem.2019.00274

Yu, M., Han, Y., Li, J., and Wang, L. (2017). CO2 -activated Porous Carbon Derived from Cattail Biomass for Removal of Malachite green Dye and Application as Supercapacitors. *Chem. Eng. J.* 317, 493–502. doi:10.1016/j.cej.2017.02.105

Yuan, Y., Sun, Y., Feng, Z., Li, X., Yi, R., Sun, W., et al. (2021). Nitrogen-doped Hierarchical Porous Activated Carbon Derived from Paddy for High-Performance Supercapacitors. *Materials* 14 (2), 318. doi:10.3390/ma14020318

Zhang, P., Xin, Y., Zhong, X., Yan, Z., Jin, Y., Yan, M., et al. (2021a). Integrated Effects of Ulva Prolifera Bloom and Decay on Nutrients Inventory and Cycling in Marginal Sea of China. *Chemosphere* 264 (1), 128389. doi:10.1016/j.chemosphere.2020.128389

Zhang, S., Shi, X., Wróbel, R., Chen, X., and Mijowska, E. (2019a). Low-cost Nitrogen-Doped Activated Carbon Prepared by Polyethylenimine (PEI) with a Convenient Method for Supercapacitor Application. *Electrochimica Acta* 294, 183–191. doi:10.1016/j.electacta.2018.10.111

Zhang, W., Xu, J., Hou, D., Yin, J., Liu, D., He, Y., et al. (2018). Hierarchical Porous Carbon Prepared from Biomass through a Facile Method for Supercapacitor Applications. *J. Colloid Interf. Sci.* 530, 338–344. doi:10.1016/j.jcis.2018.06.076

Zhang, Y., He, P., Li, H., Li, G., Liu, J., Jiao, F., et al. (2019b). Ulva Prolifera green-tide Outbreaks and Their Environmental Impact in the Yellow Sea, China. *Natl. Sci. Rev.* 6 (4), 825–838. doi:10.1093/nsr/nwz026

Zhang, Z., Liu, X., Wang, H., He, H., and Bai, R. (2021b). Preparation and Characterization of Enteromorpha Prolifera Nanocellulose/polyvinyl Alcohol Composite Films. *Polym. Composites* 42 (4), 1712–1726. doi:10.1002/pc.25926

Zhao, G., Li, Y., Zhu, G., Shi, J., Lu, T., and Pan, L. (2019). Waste Fruit Grain orange-derived 3D Hierarchically Porous Carbon for High-Performance All-Solid-State Supercapacitor. *Ionics* 25 (8), 3935–3944. doi:10.1007/s11581-019-02930-9

Zhou, M., Pu, F., Wang, Z., and Guan, S. (2014). Nitrogen-doped Porous Carbons through KOH Activation with superior Performance in Supercapacitors. *Carbon* 68, 185–194. doi:10.1016/j.carbon.2013.10.079

Zhou, Y., Tan, L., Pang, Q., Li, F., and Wang, J. (2015). Influence of Nutrients Pollution on the Growth and Organic Matter Output of Ulva Prolifera in the Southern Yellow Sea, China. *Mar. Pollut. Bull.* 95 (1), 107–114. doi:10.1016/j.marpolbul.2015.04.034

Zhu, L., Shen, F., Smith, R. L., Yan, L., Li, L., and Qi, X. (2017). Black Liquor-Derived Porous Carbons from rice Straw for High-Performance Supercapacitors. *Chem. Eng. J.* 316, 770–777. doi:10.1016/j.cej.2017.02.034

Zhu, M., Xia, A., Feng, Q., Wu, X., Zhang, C., Wu, D., et al. (2020). Biomass Carbon Materials for Efficient Solar Steam Generation Prepared from Carbonized Enteromorpha Prolifera. *Energy Technol.* 8 (5), 1901215. doi:10.1002/ente.201901215

Conflict of Interest: The authors declare that the research was conducted in the absence of any commercial or financial relationships that could be construed as a potential conflict of interest.